

## Nanostripe of subwavelength width as a switchable semitransparent mirror for spin waves in a magnonic crystal

R. Huber, T. Schwarze, and D. Grundler\*

*Lehrstuhl für Physik funktionaler Schichtsysteme, Technische Universität München (TUM), Physik Department, James-Franck-Straße 1, D-85747 Garching bei München, Germany*

(Received 21 April 2013; revised manuscript received 24 May 2013; published 18 September 2013)

Spin wave transmission experiments are performed on a one-dimensional magnonic crystal (MC) where an injection pad for domain walls reverses the magnetization  $M$  of selected nanostripes independently from the otherwise saturated MC. The MC consists of a periodic array of 255-nm-wide permalloy nanostripes with an edge-to-edge separation of 45 nm. In the experiment and simulations, we find that a single nanostripe with antiparallel  $M$  performing opposite spin precession reduces significantly the transmission of long-wavelength spin waves. Our findings allow for the implementation and current-controlled operation of magnonic devices such as spin-wave-based logic on the nanoscale.

DOI: [10.1103/PhysRevB.88.100405](https://doi.org/10.1103/PhysRevB.88.100405)

PACS number(s): 75.40.Gb, 75.30.Ds, 75.75.-c, 78.67.Pt

### I. INTRODUCTION

The control of amplitudes and phases of propagating spin waves (SWs) is of special interest for magneto-logics using SWs.<sup>1</sup> Different local inhomogeneities of magnetic properties have been explored, such as a geometric defect,<sup>2</sup> an interface,<sup>3</sup> the core polarization in nanomagnet chains,<sup>4</sup> and a local magnetic field creating a potential barrier at which reflection, transmission, and tunneling of SWs occurred.<sup>5,6</sup> Recently, it has been shown that one-dimensional (1D) magnonic crystals (MCs) consisting of interacting nanostripes allow for artificially tailored SW band structures that depend on the magnetic state.<sup>7–10</sup> For further advancements in magnonics<sup>11,12</sup> one aims at controlling spin waves with individual nanoscopic magnets.<sup>13,14</sup> In this paper, we report the control of SW propagation across a 1D array of 255-nm-wide permalloy (Ni<sub>80</sub>Fe<sub>20</sub>) nanostripes [Figs. 1(a) and 1(b)] using a deep-subwavelength magnetic element. We find a significantly reduced transmission signal when we selectively reverse one of the nanostripes in the otherwise saturated MC. Micromagnetic simulations show that a single antiparallel nanomagnet reflects a significant part of a long-wavelength SW and due to opposite spin precession provokes a switchable semitransparent mirror for SWs. The findings are relevant for SW control operated on the nanoscale in magnonic and logic applications.<sup>15,16</sup> The paper is organized as follows: In Sec. II we outline the experimental techniques and simulation parameters. Experimental data and simulation results are presented in Sec. III. We discuss the findings in Sec. IV and conclude in Sec. V.

### II. EXPERIMENTAL TECHNIQUES AND MICROMAGNETIC SIMULATIONS

The array of collinear nanostripes was structured by electron beam lithography and subsequent liftoff processing of 40-nm-thick permalloy (Py) on a GaAs substrate. The effects reported here were observed on different 1D MCs. In the following, we focus on a sample with period  $p = 300$  nm, where the edge-to-edge separation (air gap width  $\eta$ ) was 45 nm and the length of the wires amounted to about 300  $\mu\text{m}$ . Here, two selected nanostripes were attached intentionally to an injection pad (IP) for domain walls in order to

control their magnetic state independently from the remaining MC [Figs. 1(a) and 1(b)]. On top of 8-nm-thick Al<sub>2</sub>O<sub>3</sub>, coplanar waveguides (CPWs) were integrated by electron beam lithography, evaporation of Cr and Au, and liftoff processing. The widths of the signal and ground lines were 2.0  $\mu\text{m}$ . The separation between ground and signal lines was 1.3  $\mu\text{m}$ . The distance between CPW1 and CPW2 amounted to  $s_{21} = 16.5$   $\mu\text{m}$  [Fig. 1(b)]. In between them, there were the two nanostripes attached to the IP covered by CPW3. By a vector network analyzer (VNA) we applied an rf electromagnetic wave to one of the CPWs. The magnetic rf field  $\mathbf{h}_{\text{rf}}$  excited the magnetization  $\mathbf{M}$  of nearby nanostripes via the torque  $\tau = d\mathbf{M}/dt \propto -\mathbf{M} \times \mathbf{h}_{\text{rf}}$  ( $t$  is the time) as extracted from the Landau-Lifshitz equation.<sup>3</sup> Using the VNA we measured scattering parameters  $S_{ij}$  ( $i, j = 1, 2, 3$  label the three CPWs), where  $j$  indicates the emitter CPW for SWs and  $i$  the detector CPW.<sup>17,18</sup> The CPWs provoked a maximum of spin wave excitation near wave vector  $k = 2\pi/\lambda \simeq 0.5 \frac{1}{\mu\text{m}}$  collinear with the  $x$  direction (the wavelength is  $\lambda \simeq 12 \mu\text{m} \gg p$ ). A magnet provided in-plane fields  $H$  along the  $y$  direction [Fig. 1(b)]. We took a reference data set  $S_{ij}(\text{Ref})$  which was subtracted from the raw data  $S_{ij}(H)$  to extract the magnetic response  $a_{ij} = S_{ij}(H) - S_{ij}(\text{Ref})$ . For  $S_{ij}(\text{Ref})$ ,  $\mu_0 H = 100$  mT was applied perpendicular to the CPW, thereby reducing  $\tau$  significantly and avoiding pronounced absorption by SWs. We denote  $\text{Re}(a_{ij})$  and  $\text{Im}(a_{ij})$  as the real and imaginary part of  $a_{ij}$ , respectively, and  $\text{Mag}(a_{ij})$  as the magnitude. The quantity  $a_{ij}$  reflects the susceptibility. Magnetic states of nanostripes were investigated by a magnetic force microscope (MFM). Micromagnetic simulations were performed using the commercial software MICROMAGUS<sup>19</sup> using standard parameters for permalloy.<sup>20</sup> We simulated propagating spin waves after a pulsed excitation following Ref. 3.

### III. EXPERIMENTAL DATA AND SIMULATION RESULTS

#### A. Broadband spin wave spectroscopy

SW resonances (dark) measured separately on the 1D MC via CPW1 and injection pad via CPW3 are shown in Figs. 1(c) and 1(d), respectively. First a saturation field of  $\mu_0 H_{\text{sat}} = +100$  mT was applied. Then  $H$  was decreased in

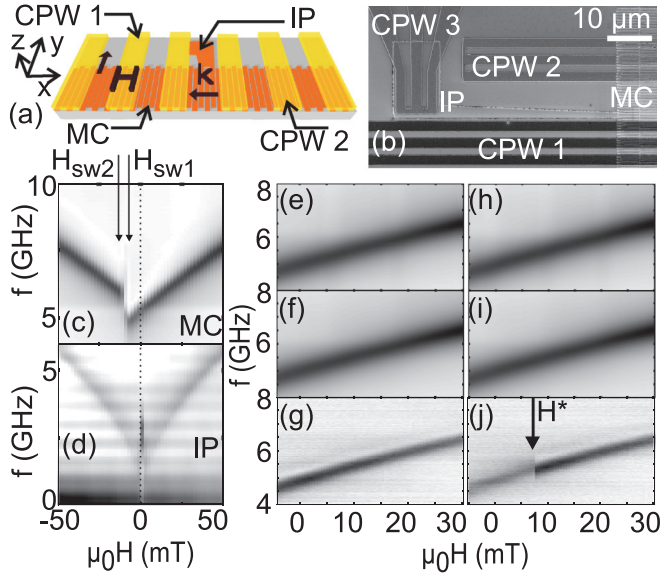


FIG. 1. (Color online) (a) Sketch of the nanostructure array and (b) scanning electron microscopy image showing coplanar waveguides CPW1, CPW2, and CPW3. Two nanowires are connected to an injection pad (IP). (c) Signal  $\text{Mag}(a_{11})$  and (d)  $\text{Mag}(a_{33})$  from CPW1 and CPW3 detecting the MC and the IP, respectively. The reversal of the MC (IP) is observed between fields  $H_{sw1}$  and  $H_{sw2}$  i.e.  $-12 \pm 1 < \mu_0 H < -8 \pm 1$  mT (at  $\mu_0 H = 1 \pm 1$  mT). Spectra obtained in a minor loop (ML) with  $\mu_0 H_{ML} = -4$  mT addressing the ferromagnetically ordered state: (e)  $\text{Mag}(a_{11})$ , (f)  $\text{Mag}(a_{22})$ , and (g)  $\text{Mag}(a_{21})$ . Spectra obtained for  $\mu_0 H_{ML} = -5$  mT: (h)  $\text{Mag}(a_{11})$ , (i)  $\text{Mag}(a_{22})$ , and (j)  $\text{Mag}(a_{21})$ . In the transmission signal  $\text{Mag}(a_{21})$ , the signal strength varies abruptly at  $\mu_0 H^* = 7.5$  mT.

a stepwise manner, and spectra were recorded. Overall, the eigenfrequencies  $f$  of the MC and IP differ by about 2 GHz due to different shape anisotropies. The monotonous behavior of the branches is interrupted at switching fields  $H_{sw}$ . For the MC we define two values  $\mu_0 H_{sw1} = -8 \pm 1$  mT and  $\mu_0 H_{sw2} = -12 \pm 1$  mT reflecting the switching field distribution of the nanostripes.<sup>7,9</sup> In the 1D MC, the main resonance is given by the  $n = 0$  mode where  $n$  counts the number of nodal lines in the spin precessional motion of a single nanostripe.<sup>21</sup> Abrupt changes in eigenfrequency are due to the successive reversal of nanostripes.<sup>9</sup> For  $H_{sw2} < H < H_{sw1}$ , the magnetic state  $\mathbf{M}(\mathbf{r})$  thus deviates from a saturated state polarized along the  $y$  axis. For the  $200 \mu\text{m}^2$  large injection pad (CPW3), we find a single-valued switching field  $\mu_0 H_{sw,IP} = 1 \pm 1$  mT. Here, we assume domain wall nucleation and movement as the relevant reversal mechanism. The injection pad is thus expected to inject domain walls into the attached nanostripes. If the injection occurred for  $\mu_0 H_{sw1} = -8$  mT  $< \mu_0 H < 1$  mT, these nanostripes would have  $\mathbf{M}$  antiparallel to the otherwise saturated 1D MC.

In Fig. 1(e) we depict  $\text{Mag}(a_{11})$  measured in a minor loop (ML) on CPW1. The saturation field was  $\mu_0 H_{sat} = +100$  mT before we applied  $\mu_0 H_{ML} = -4$  mT and measured for increasing  $H$ . As  $\mu_0 H_{ML} > \mu_0 H_{sw1}$  the reversal of nanostripes without injection pad was not initiated. Nanostripes have all a parallel magnetization  $\mathbf{M}$  and form the ferromagnetically ordered (FMO) state of the 1D MC.<sup>7</sup> We detect the same continuous branch  $f(H)$  for  $\text{Mag}(a_{22})$  on CPW2 [Fig. 1(f)].

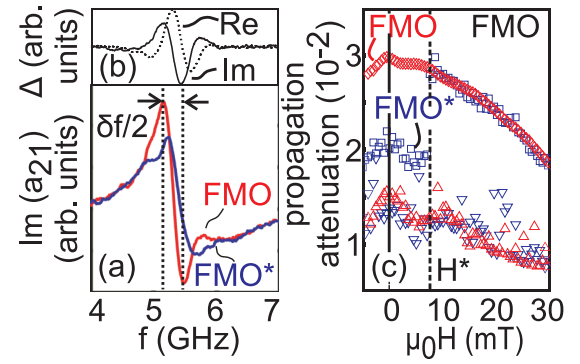


FIG. 2. (Color online) (a) Transmission signals  $\text{Im}(a_{21})$  of FMO and FMO\* states.  $\delta f$  is a measure of  $v_g$ . (b)  $\text{Im}(\Delta) = \text{Im}[a_{21}(\text{FMO})] - \text{Im}[a_{21}(\text{FMO}^*)]$  (line)  $[\text{Re}(\Delta) = \text{Re}[a_{21}(\text{FMO})] - \text{Re}[a_{21}(\text{FMO}^*)]]$  (dotted) where oscillating behaviors indicate propagating spin waves. (c) Propagation attenuation  $\text{Mag}(a_{21})/\text{Mag}(a_{11})$  and  $\text{Mag}(a_{12})/\text{Mag}(a_{22})$  for the FMO (diamond and upward triangle, respectively) and FMO\* state (square and downward triangle, respectively). For  $H > H^*$ , the FMO state exists.

For  $\text{Mag}(a_{21})$  in Fig. 1(g), i.e., the signal transmitted between CPW1 and CPW2 in the  $x$  direction, a branch is seen at the same field-dependent eigenfrequencies as in Figs. 1(e) and 1(f). The transmission signal does not show abrupt changes either in frequency  $f$  or in signal strength. In Figs. 1(h) and 1(i),  $\text{Mag}(a_{11})$  and  $\text{Mag}(a_{22})$  are shown for  $\mu_0 H_{ML} = -5$  mT. The branches are identical to Figs. 1(e) and 1(f), respectively. The transmission signal  $\text{Mag}(a_{21})$  in Fig. 1(j) displays however an abrupt change of signal strength at  $\mu_0 H^* = 7.5$  mT. For  $\mu_0 H < 7.5$  mT ( $\mu_0 H > 7.5$  mT) the detected signal is weak (strong). This observation is attributed to a field-induced variation of the magnetic state  $\mathbf{M}(\mathbf{r})$  specifically between CPW1 and CPW2. The antiparallel  $\mathbf{M}$  of a nanostripe attached to the IP will be substantiated later by the MFM. We label the relevant state between  $\mu_0 H_{ML} = -5$  mT and  $\mu_0 H^* = 7.5$  mT in Fig. 1(j) as the “ferromagnetically ordered state with a magnetic defect (FMO\*).”

We now study in detail the propagation properties of spin waves below and above  $H^*$  for the FMO and FMO\* states. Figure 2(a) shows a direct comparison of  $\text{Im}(a_{21})$  taken at  $\mu_0 H = 7.0$  mT for FMO and FMO\*. Both states show a transmission signal near the eigenfrequency  $f = 5.5$  GHz. The signals differ considerably in shape and amplitude though they are taken at the same field  $H$  and  $\mu_0 H_{ML}$  is varied by only 1 mT [cf. Figs. 1(e) to 1(j)]. In the FMO state, the curve contains a clearly oscillatory part which is known to indicate spin wave propagation between emitter and detector.<sup>18</sup> In the FMO\* state, the oscillatory contribution is weaker. We now subtract the two curves to reduce the background.<sup>22</sup> The phase-shifted oscillatory behaviors of  $\text{Im}(\Delta) = \text{Im}(a_{21})(\text{FMO}) - \text{Im}(a_{21})(\text{FMO}^*)$  (line) and  $\text{Re}(\Delta) = \text{Re}(a_{21})(\text{FMO}) - \text{Re}(a_{21})(\text{FMO}^*)$  (dotted) in Fig. 2(b) indicate a VNA-measured SW propagation signal in an ideal way.<sup>18</sup> Following the subtraction, the transmission of SWs is reduced for the FMO\* compared to the FMO state. The group velocity extracted from  $\delta f$  amounts to  $v_g = \delta f \times s_{21} = 4.6$  km/s. In Fig. 2(c), the field-dependent propagation attenuation  $\text{Mag}(a_{21})/\text{Mag}(a_{11})$  is shown.<sup>10</sup> For the FMO state,  $\text{Mag}(a_{21})/\text{Mag}(a_{11})$  (open diamonds) decreases for increasing

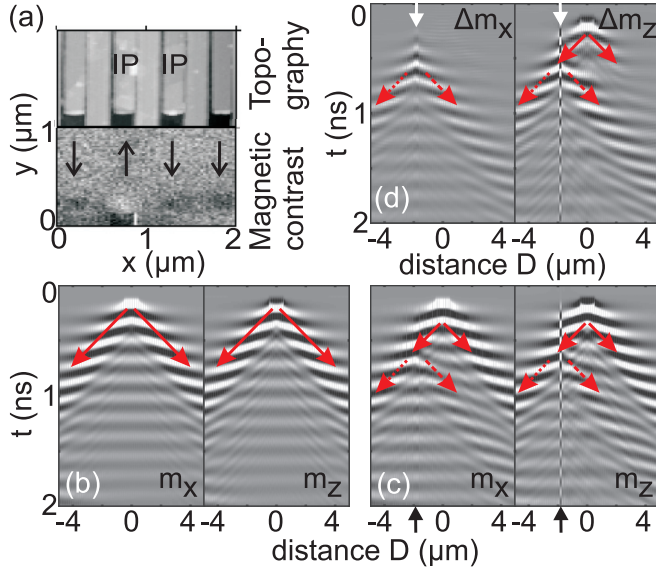


FIG. 3. (Color online) (a) MFM image for the two nanostripes connected to the injection pad as indicated. Every second nanostripe is intentionally a little bit longer. The topography (top) and the stray-field contrast (bottom) are shown. Dark (light) contrast indicates a magnetization  $\mathbf{M}$  (arrow) in  $+y$  direction ( $-y$  direction). One nanostripe with injection pad is found in a reversed state (white end) for  $\mu_0 H_{sw1} < \mu_0 H_{ML} < 0$ . (b) Simulated in-plane  $m_x$  and out-of-plane  $m_z$  component of  $\mathbf{m}(x, z, t)$  for the FMO state at  $H = 0$ . Spin waves propagate in both directions (solid arrows). (c)  $m_x$  and  $m_z$  for FMO\* with one nanostripe of antiparallel  $\mathbf{M}$  at  $-1.9 \mu\text{m}$  (vertical arrows). A reflected (dashed arrow) and transmitted (dotted arrow) wave is seen.  $m_x$  ( $m_z$ ) of the MD oscillates in-phase (out-of-phase) with the MC. (d) Difference between (b) and (c) highlighting the MD-induced effects.

$H$  starting from a value of about 0.03. Strikingly for the FMO\* state,  $\text{Mag}(a_{21})/\text{Mag}(a_{11})$  (open squares) starts at a low level of 0.02 and exhibits an abrupt jump to larger values at  $H^*$ . For  $H > H^*$ ,  $\text{Mag}(a_{21})/\text{Mag}(a_{11})$  of FMO\* recovers the values of the FMO state perfectly. Note that  $\text{Mag}(a_{12})/\text{Mag}(a_{22})$  measured in the opposite propagation direction [open upward (FMO) and downward (FMO\*) triangles] is found at very small values for both magnetic states due to the nonreciprocal SW excitation.<sup>10,23</sup> The discrepancy between FMO and FMO\* states can thus not be resolved with the same signal-to-noise ratio. In the following we first investigate the magnetic state  $\mathbf{M}(\mathbf{r})$  of the MC by an MFM and second perform micromagnetic simulations.

### B. Magnetic force microscopy

For each MFM data set the MC was first saturated at large  $\mu_0 H_{\text{sat}}$  of about +100 mT. The field was passed through zero reaching  $\mu_0 H_{ML} < 0$  and then gradually increased. The MFM images were taken at  $H = 0$ . Reference MFM images with  $\mu_0 H_{\text{sat}} \approx +100$  mT ( $\mu_0 H_{\text{sat}} \approx -100$  mT) and  $\mu_0 H_{ML} = 0$  provided all black (white) contrast at a given end of the nanostripes (not shown). Applying  $H_{sw1} < H_{ML} < 0$ , we detected the reversal of one nanostripe (white) in Fig. 3(a) (bottom graph).<sup>24</sup> Comparing with the topography image taken with the MFM (top graph), we substantiated that the

reversed nanostripe was attached to the IP. We did not detect the white color for both nanostripes at the same time for  $H_{sw1} < H_{ML} < 0$ . There might have been a pinning potential along the second nanostripe attached to the injection pad preventing this particular nanostripe from a full reversal at such small  $|H_{ML}| < |H_{sw1}|$ . The FMO\* state is thus argued to contain a single magnetic nanostripe of opposite  $\mathbf{M}$ .

### C. Simulated spin wave propagation

In Figs. 3(b) to 3(d) we depict the outcome of the micromagnetic simulations. We simulated an array consisting of 256 nanostripes with a period  $p = 300$  nm and a length of  $4.8 \mu\text{m}$  each. The length was smaller than in the experiment due to restrictions existing with nowadays computational power. On the vertical axis of Fig. 3(b) from top to bottom we follow the temporal evolution of the dynamical magnetization  $\mathbf{m}(x, z, t)$  of nanostripes after application of a field pulse at  $t = 0$ . We depict the components  $m_x$  (left) and  $m_z$  (right). The  $x$  axis shows the distance  $D$  measured to both sides from the excited nanostripes located at  $D = 0$ . We observe spin-wave packets as they move to both sides of the 1D MC (highlighted by two arrows). The black and white contrast of the ringing pattern illustrates negative and positive spin-precessional amplitudes, respectively. To achieve a large signal-to-noise ratio up to  $|D| = 4 \mu\text{m}$  and thereby illustrate the underlying physics clearly we provoked a large  $v_g$  by considering a small air gap width of  $\eta = 9$  nm in the simulation.<sup>25</sup>

In Fig. 3(c), simulation data for the FMO\* state are displayed for  $H = 0$  where at  $D = -1.9 \mu\text{m}$  a single nanostripe with an antiparallel magnetization  $\mathbf{M}$  is included. At this magnetic defect (MD), a SW (solid arrow) splits into a reflected (dashed arrow) and transmitted wave (dotted arrow) that experiences a reduced amplitude consistent with our experimental observation. We now subtract the simulated traces for FMO and FMO\* providing  $\Delta m_x$  and  $\Delta m_z$  in Fig. 3(d). For  $\Delta m_x$  only the transmitted and reflected SW beams are visible. The spin-precessional amplitudes suggest efficient SW reflection at the single magnetic nanoelement (about 50%). The MD shows a ringing pattern being *in-phase* with the spin waves. For  $\Delta m_z$  in Fig. 3(d), the incoming SW is visible for about  $-2 \mu\text{m} < D < 2 \mu\text{m}$ . This is attributed to the dipolar interaction of nearby nanostripes with the MD modifying their ellipticity  $\frac{m_z}{m_x}$ . Strikingly, for  $\Delta m_z$  the ringing of the MD is  $\pi$ -phase-shifted with respect to the neighboring MC.

## IV. DISCUSSION

To analyze in detail the spin-precessional motion we subdivide  $\mathbf{M}$  of a nanostripe into a static component  $\mathbf{M}_y$  collinear with the  $y$  axis and a dynamic component  $\mathbf{m}$  precessing in the  $x, z$  plane according to  $\mathbf{M} = \mathbf{M}_y + \mathbf{m}_{x,z}$  ( $m_{x,z} \ll M_y$ ). Excitation of neighboring stripes is provoked by dynamic demagnetizing fields  $\mathbf{h}_d(\mathbf{r}) = \int_V \hat{G}(\mathbf{r}, \mathbf{r}') \mathbf{m}(\mathbf{r}') d\mathbf{r}'$ , where  $\hat{G}$  is the tensorial magnetostatic Green's function and  $\mathbf{r}, \mathbf{r}'$  are position vectors inside and outside the nanostripes of volume  $V$ . For the FMO state all nanostripes have  $+M_y$ , and neighboring nanostripes precess in unison in a *right-handed* manner around the  $+y$  direction. Following  $\tau \propto -\mathbf{M} \times \mathbf{h}_d$ , a strong in-plane component  $+h_{d,x}$  deflects neighboring stripes

in the same manner for  $\lambda \gg p$ , such that their dynamic components  $\mathbf{m}$  point, e.g., into the  $-z$  direction at the same time. Consequently,  $h_{d,z}$  is large and the same for neighboring stripes. In contrast, in the FMO\* state  $\mathbf{M}$  of the MD exhibits  $-M_y$  and performs a *left-handed* precession under excitation of  $+h_{d,x}$ . Following Ref. 7, the component  $m_{MD,x}$  of mode  $n = 0$  can still be in-phase with the MC for  $\lambda \gg p$ , but  $\mathbf{m}_{MD}$  precesses towards the  $-z$  direction while neighboring unit cells of the MC precess towards the  $+z$  direction. Thereby, the MD experiences a partly compensated demagnetization field and different  $\tau$  compared to the FMO state. This difference provokes a mismatched “wave impedance” for the SW leading to partial reflection and reduced transmission at the subwavelength-wide magnet ( $w/\lambda \approx 0.02-0.03$ ). Note that the “wave impedance mismatch” is due to the counterprecessing  $\mathbf{m}_{MD}$  of a single nanomagnet in contrast to the local inhomogeneities exploiting a SW band structure mismatch so far.<sup>2,3,5,6</sup> The magnonic crystal with periodic nanopatterning is key to provoke the observed type of elastic scattering. In further simulations we have considered different numbers  $q$  of selectively reversed nanostripes (we tested  $q = 1, 2, 3, 4$ ). The reflected SW intensity did not depend crucially on  $q$  suggesting an “interfacial” rather than a “bulklike” effect. The discovered semitransparent SW mirror is far reaching. It has been shown that  $\mathbf{M}$  of a stripe can be reversed by a biasing current which moves back and forth an existing domain wall.<sup>26</sup>

By integration of leads, a three-terminal 1D MC with emitter and detector antennas can be created where a central nanostripe is controlled by current pulses.<sup>27</sup> Then, the transmitted SWs can be switched between high and low signal levels consistent with transistor applications in digital electronics. Using two of the mirrors in series, spin wave cavities in MCs<sup>2</sup> become switchable.

## V. CONCLUSIONS

In conclusion, we studied spin wave propagation in 1D MCs with a reprogrammable magnetic defect. The spin wave was partially reflected at the single subwavelength nanostripe with antiparallel magnetization due to out-of-phase precession. Such a semitransparent mirror can be switched on and off by the magnetic history or a current offering spin wave control on the nanoscale.

## ACKNOWLEDGMENTS

We thank M. Becherer and the European Community’s Seventh Framework Programme (FP7/2007-2013) for funding under Grant No. 228673 (MAGNONICS), the TUM Institute for Advanced Study funded by the German Excellence Initiative, and the German Excellence Cluster Nanosystems Initiative Munich (NIM).

\*grundler@ph.tum.de

<sup>1</sup>T. Schneider, A. A. Serga, B. Leven, B. Hillebrands, R. L. Stamps, and M. P. Kostylev, *Appl. Phys. Lett.* **92**, 022505 (2008).

<sup>2</sup>Y. Filimonov, E. Pavlov, S. Vystostkii, and S. Nikitov, *Appl. Phys. Lett.* **101**, 242408 (2012).

<sup>3</sup>S. Neusser, H. G. Bauer, G. Duerr, R. Huber, S. Mamica, G. Woltersdorf, M. Krawczyk, C. H. Back, and D. Grundler, *Phys. Rev. B* **84**, 184411 (2011).

<sup>4</sup>S. Barman, A. Barman, and Y. Otani, *J. Phys. D: Appl. Phys.* **43**, 335001 (2010).

<sup>5</sup>T. Neumann, A. A. Serga, B. Hillebrands, and M. P. Kostylev, *Appl. Phys. Lett.* **94**, 042503 (2009).

<sup>6</sup>S. O. Demokritov, A. A. Serga, A. André, V. E. Demidov, M. P. Kostylev, B. Hillebrands, and A. N. Slavin, *Phys. Rev. Lett.* **93**, 047201 (2004).

<sup>7</sup>J. Topp, D. Heitmann, M. P. Kostylev, and D. Grundler, *Phys. Rev. Lett.* **104**, 207205 (2010).

<sup>8</sup>S. Tacchi, M. Madami, G. Gubbiotti, G. Carlotti, S. Goolaup, A. O. Adeyeye, N. Singh, and M. P. Kostylev, *Phys. Rev. B* **82**, 184408 (2010).

<sup>9</sup>J. Ding, M. Kostylev, and A. O. Adeyeye, *Phys. Rev. Lett.* **107**, 047205 (2011).

<sup>10</sup>R. Huber, M. Krawczyk, T. Schwarze, H. Yu, G. Duerr, S. Albert, and D. Grundler, *Appl. Phys. Lett.* **102**, 012403 (2013).

<sup>11</sup>V. V. Kruglyak, S. O. Demokritov, and D. Grundler, *J. Phys. D: Appl. Phys.* **43**, 264001 (2010).

<sup>12</sup>B. Lenk, H. Ulrichs, F. Garbs, and M. Münzenberg, *Phys. Rep.* **507**, 107 (2011).

<sup>13</sup>R. Hertel, W. Wulfhekel, and J. Kirschner, *Phys. Rev. Lett.* **93**, 257202 (2004).

<sup>14</sup>Y. Au, E. Ahmad, O. Dmytriiev, M. Dvornik, T. Davison, and V. V. Kruglyak, *Appl. Phys. Lett.* **100**, 182404 (2012).

<sup>15</sup>A. Khitun, M. Bao, and K. L. Wang, *J. Phys. D: Appl. Phys.* **43**, 264005 (2010).

<sup>16</sup>J. Ding and A. Adeyeye, *Appl. Phys. Lett.* **101**, 103117 (2012).

<sup>17</sup>M. Bailleul, D. Olligs, C. Ferman, and S. O. Demokritov, *Europhys. Lett.* **56**, 741 (2001).

<sup>18</sup>V. Vlaminck and M. Bailleul, *Phys. Rev. B* **81**, 014425 (2010), and references therein.

<sup>19</sup>D. V. Berkov and N. L. Gorn, MICROMAGUS, software for micro-magnetic simulations, <http://www.micromagus.de>.

<sup>20</sup>Parameters were cell size  $9 \times 9 \times 40 \text{ nm}^3$ , 256 stripes, stripe length  $4.8 \mu\text{m}$ , stripe width 291 nm, air gap width  $\eta = 9 \text{ nm}$ , saturation magnetization 820 kA/m, exchange constant  $1.3 \times 10^{-6} \text{ ergs/cm}$ , damping constant 0.005, open boundary conditions, Gaussian-shaped excitation pulse of duration 0.1 ns.

<sup>21</sup>J. Topp, G. Duerr, K. Thurner, and D. Grundler, *Pure Appl. Chem.* **83**, 1989 (2011).

<sup>22</sup>The detailed curve shapes in Fig. 2(a) indicate that we have both a propagating spin wave signal and direct electromagnetic (em) crosstalk between CPW1 and CPW2 (steplike feature between 4 and 7 GHz). The difference signal  $\Delta$  does not contain the em crosstalk.

<sup>23</sup>M. Kostylev, *J. Appl. Phys.* **113**, 053907 (2013).

<sup>24</sup>The MFM setup was not calibrated with the same Hall sensors incorporated in the spectroscopy setup, and absolute field values

$H_{ML}$  therefore did not agree perfectly between the two setups.  $H_{sw1}$  is extracted at the MFM from the reversal of nanostripes *not connected* to the IP.

<sup>25</sup>Though  $\eta$  differs between simulation and experiment, extracted velocities  $v_g$  are found to be nearly the same. Unintentional edge roughness in the real nanostripes might be the reason. Roughness is known to reduce the demagnetization effect and thereby enhances

spin-precessional amplitudes right at the geometrical edges provoking a large  $v_g$  via enhanced dipolar coupling.

<sup>26</sup>A. Yamaguchi, T. Ono, S. Nasu, K. Miyake, K. Mibu, and T. Shinjo, *Phys. Rev. Lett.* **92**, 077205 (2004).

<sup>27</sup>Y. Togawa, T. Kimura, K. Harada, A. Tonomura, and Y. Otani, *J. Phys. D: Appl. Phys.* **44**, 064015 (2011).